Spanish Journal of Agricultural Research
17 (2), e0202, 15 pages (2019)
eISSN: 2171-9292
https://doi.org/10.5424/sjar/2019172-13886
Instituto Nacional de Investigación y Tecnología Agraria y Alimentaria, O.A, M.P. (INIA)

RESEARCH ARTICLE

OPEN ACCESS

X-ray computerized tomography for characterization of pick-up destruction and pick-up parameter optimization of tomato root lumps

Hanping Mao[1,2], Yang Liu[1,3], Luhua Han[1,2], Baoguo Sheng[1,2], Guoxin Ma[1,2] and Yaxiong Li[3]

[1]Key Laboratory of Modern Agriculture Equipment and Technology, Ministry of Education, Jiangsu University, Zhenjiang, Jiangsu 212013, China. [2]High-tech Key Laboratory of Agricultural Equipment & Intelligentization of Jiangsu Province, Jiangsu University, Zhenjiang, Jiangsu 212013, China. [3]Mechanical Equipment Research Insistute, Xinjiang Academy of Agricultural and Reclamation Science, Shihezi, Xinjiang 832000, China.

Abstract

This study was aimed to find the causes of pick-up destruction of tomato root lumps using X-ray microcomputed tomography, and to identify the pick-up parameters of low root lump destruction. The roots and pores were reconstructed three-dimensionally and analyzed quantitatively. It was found that the roots acted winding and wraping the root lumps and thus preventing the substrate from loosening. The major causes for root lump destruction were pore aggregation and crack formation. The apex and circumference of pick-up pins were areas where root lumps were prone to fracture and breakage, respectively. Lacunarities of these two areas were used as index to quantify the root lump destruction. Single-factor analysis of variance was conducted with pick-up pin shape (circular, flat), diameter (2, 2.5, 3 mm) and initial pick-up angle (18°, 21°, 24°) as the test factors and then the effects of these three factors on root lump destruction were studied. It was found the lacunarities at the fracturable area and breakable area both increased with the rise of pick-up pin diameter and decreased with the rise of initial pick-up angle. At the same pick-up conditions, lacunarities with the use of flat pins always surpassed that of circular pins. When circular pick-up pins with diameter of 2 mm and initial pick-up angle of 24° were used, the destruction rate of root lumps (6.63%) was smaller than under other test conditions. The optimized pick-up parameters can be used to guide gripper design and to improve the working performance of automatic transplanters.

Additional keywords: damage; roots; pore distribution; fractal dimension; crack.

Abbreviations used: CT (computerized tomography); μCT (microcomputed tomography); *d* (pin diameter); D_{PH} (horizontal lacunarity); D_{PV} (vertical lacunarity); D_{PD} (lacunarity in the fracturable zone); D_{PS} (lacunarity at the breakable zone); D_{RH} (horizontal root distribution density); D_{RV} (vertical root distribution density); F_{PH} (horizontal pore fractal dimension); F_{PV} (vertical pore fractal dimension); IPL (image processing language); V_{RH} (horizontal root volume); V_{RV} (vertical root volume); θ (initial pick-up angle).

Authors' contributions: Conceived, designed and performed the experiments: HPM, YL, LHH and BGS. Analyzed the data: HPM, YL and YXL. Contributed reagents/materials/analysis tools: HPM, YL and GXM. Wrote the paper: HPM and YL. All authors read and approved the final manuscript.

Citation: Mao, H. P.; Liu, Y.; Han, L. H.; Sheng, B. G.; Ma, G. X.; Li, Y. X. (2019). X-ray computerized tomography for characterization of pick-up destruction and pick-up parameter optimization to tomato root lumps. Spanish Journal of Agricultural Research, Volume 17, Issue 2, e0202. https://doi.org/10.5424/sjar/2019172-13886

Received: 02 Sep 2018. **Accepted:** 25 Jun 2019.

Funding: National Scientists Foundation of China (51475216); National Key Research and Development Program of China (2017YFD0700805-3); Open Fund of the Ministry of Education Key Laboratory of Modern Agricultural Equipment and Technology & High-tech Key Laboratory of Agricultural Equipment and Intelligentization of Jiangsu Province (NZ201607); Jiangsu Province Key Research and Development Program of China (BE2017303); Innovation Project of Science & Technology for College Graduates of Jiangsu Province (KYZZ16_0329).

Competing interests: The authors have declared that no competing interests exist.

Correspondence should be addressed to Hanping Mao: qtragr@163.com

Introduction

Tomato seedling transplant can increase yield and economic benefits and thus has been widely applied in China (Kumi *et al.*, 2016). Semi-automatic transplanters are commonly used, but at low transplanting efficiency (Kumar & Raheman, 2008); automatic transplanters are relatively more efficient, but due to technical limitations, their grippers cannot reliably pick up tomato plug seedlings from the seedling trays and severely destroy the root lumps during the pick-up process, which reduce the success rate and yield of tomato plug seedlings after the transplantation (Hu *et al.*, 2014; Jin *et al.*, 2015).

Choi *et al.* (2012) studied the seedling substrate composition and water-fertilizer management methods that are suitable for vegetable seedling transplantation and planting. Fukushima *et al.* (2012) investigated the relationship between the shape of cabbage plug seedlings and the transplanting quality. Kumi *et al.* (2016)

characterized the growth of tomato plug seedlings under different seedling substrate compositions. In the above three studies, the problem of root lump damage during automatic seedling pick-up was solved by improving the seedling quality. Ryu *et al.* (2001) experimentally studied seedling pick-up by using grippers of different shapes. Mao *et al.* (2014) designed a two-finger four-pin gripper and studied the relationships of seedling pick-up success rate with inserted depth of pick-up pin into root lumps, pick-up force, and plug seedling age. Tong *et al.* (2014) tested the pick-up force of cucumber plug seedlings by considering pick-up pin diameter, pick-up pin number, root lump water content, and substrate composition as test factors. Han *et al.* (2015) studied the relationships of seedling pick-up success rate with the inserting speed and picking-up speed of gripper over plug seedlings. Jiang *et al.* (2017) designed a slip-pin gripper and tested seedling pick-up using root lump water content, density, and substrate composition as test factors. These studies were focused on how to take out seedlings from the trays and to put them into the planting part, but ignored the effects of pick-up parameters on root lump damage, the key deciding factor of transplant failure.

When a gripper picks up a root lump, damage occurs inside the lump, so the newly-formed pores and cracks cannot be observed. So far, there is scarce research on the occurrence of catch-up destruction inside root lumps during automatic pick-up of plug seedlings (Choi *et al.*, 2002; Han *et al.*, 2013). With the development of imaging technology, such as X-ray microcomputed tomography (μCT), researchers are able to visualize in-situ the structural characteristics of roots and pores in a non-destructive way. μCT has been increasingly applied into agricultural engineering (Mooney *et al.*, 2012; Stefan *et al.*, 2015).

This study was aimed to nondestructively detect tomato root lumps using X-ray μCT, extract and three-dimensionally reconstruct the roots and pores inside root lumps, quantitatively analyze the distributions of roots and pores during the picking-up, and optimize the pick-up parameters of reducing destruction to root lumps. This study theoretically underlies the design of automatic transplanter gripper and the selection of pick-up parameters.

Material and methods

Preparation of tomato plug seedling specimens

Tomato seedlings were cultivated in 128-pore plastic trays (16×8); the pores were shaped like an inversed quadrangular platform and their sizes were: upper width = 30 mm, lower width = 13 mm, height = 40 mm; included angle between two face-to-face walls = 24°; volume = 19.45 cm^3. The seedling substrate was a mixture of sphagnum peat moss, perlite and vermiculite (3:1:1 v/v/v); the trays were filled with the substrate at the 1.2-fold volume of pores (Kumar & Raheman, 2010; Nandede *et al.*, 2014). Xinken 84-7 tomato seeds were embedded at the depth of 5 mm and cultivated in a modern greenhouse at Jiangsu University for a growth cycle of 45 days.

Instruments

The tomato root lumps were scanned by an X-ray μCT 100 instrument (SCANCO Medical AG, Switzerland) in the Key Laboratory of Modern Agricultural Equipment and Technology, Jiangsu University. The X-ray μCT scanner had the operating system OVDM (Open VMS /DEC windows Motif 1.1, designed by SCANCO Medical AG) and image processing language (IPL) that can be used to three-dimensionally reconstruct the roots and pores and to measure the volume and distance between two random points in space.

During the trials, the tomato plug seedling and the pick-up device must be put into a barrel-shaped container (diameter = 100 mm, height = 120 mm) (Fig. 1). The pick-up arm and the pick-up pin formed a gripper. Then the position-regulating hob was rotated, so two grippers could transversally contract or stretch in a symmetrical

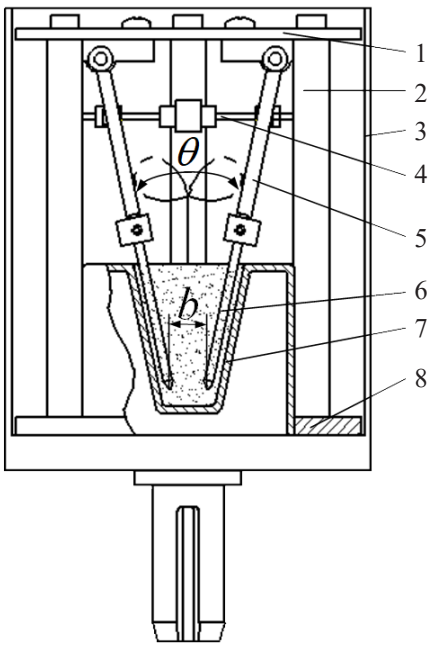

Figure 1. The pick-up device for scanning tomato root lumps via μCT. 1: cover board; 2: supporting shore; 3: specimen container; 4: position-regulating hob; 5: pick-up arm; 6: pick-up pin; 7: seedling box; 8: foundation.

way, and the pick-up arms could be installed with pick-up pins of different shapes. Generally, pick-up pins are metal-made; in order to avoid metal artifacts during scanning (Kalender *et al.*, 1987; Roberson *et al.*, 1997), we used pick-up pins made of glass fibers and in density of 2.08 g/cm^3. The foundation, supporting shore and cover board of the pick-up device were made of polyvinyl chloride.

To accurately control the initial pick-up angle θ and contraction *b* when pick-up pins are inserted into a root lump, we made seedling boxes to hold the plug seedlings (Fig. 1). The pores in the seedling boxes for placement of root lumps were of the same sizes as the 128-pore seedling trays. The wall thickness and density of the boxes were 2 mm and 1.01 g/cm^3, respectively.

Setting of scanning parameters

During scanning, the μCT parameters were set as: voltage = 45 Kvp, current = 75 μa, resolution = 50 μm, integral time interval = 400 ms; the signals were denoised using an AL0.1 filter (Zappala *et al.*, 2013a). To study the pore distribution on CT graphs at different pick-up states, we set the same initial reference line for each scan. The water content of root lumps would affect the clearness of 3D root reconstruction, and Zappala *et al.* (2013b) found the root extraction clearness was the optimal when the soil water content in scanning ripe seedlings was 25-35%. In our study, we set the water contents of tomato root lumps to be 30-35%, at which the root lump density was 1.72 g/cm^3.

3D reconstruction of roots and pores

When the water content of tomato root lumps is 30-35% (Fig. 2A), the densities of sphagnum peat moss and perlite are 1.65 and 1.57 g/cm^3, respectively, which are very similar. The very low contrast on the CT graphs of root lumps (Fig. 2B) makes them hardly distinguishable. On the contrary, the vermiculite with higher density (2.01 g/cm^3) than the other two components is very bright. On the CT graphs, the main roots and pores can be clearly located, so closed boundary lines around the main roots and pores were plotted separately. The threshold of the selected zone can be read in the Open VMS/DECwindows Motif 1.1 (OVDM) system. Thresholds of the main roots and pores were determined separately from multiple CT graphs and then averaged. The final thresholds of roots and pores were 64-73 and 0-15, respectively. Then with the threshold partition command on IPL, the roots and pores were extracted and three-dimensionally reconstructed (Fig. 2C, 2D). However, the 3D root images also showed some substrate grains, but did not show a part of fine lateral roots. This was because the root and seedling substrate could not be fully differentiated due to their low contrast on the CT images (Mooney *et al.*, 2012; Stefan *et al.*, 2015) and the scanning resolution could also affect the quality of root reconstruction (Richard *et al.*, 2012; Saoirse *et al.*, 2013).

To validate the precision of root segmented extraction, we first measured the extracted root volume to

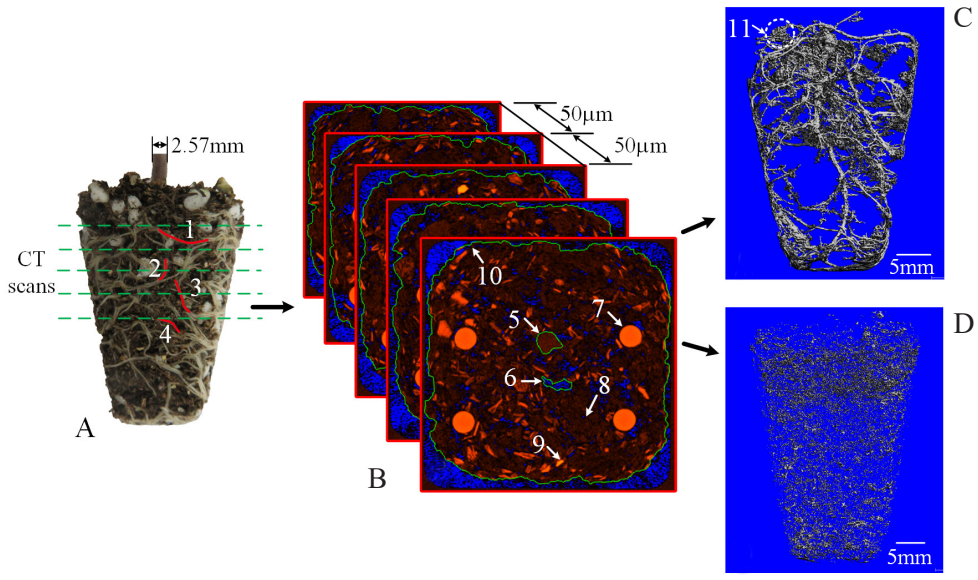

Figure 2. Tomato root lumps (A) and CT graphs (B); 3D graphs of roots (C) and pores (D) after threshold segmentation and reconstruction. 1, 2, 3 and 4: lateral roots for distance measurement; 5: main roots and boundary lines; 6: pores and boundary lines; 7: pick-up pins; 8: sphagnum peat moss and perlite; 9: vermiculite; 10: root lump and boundary lines; 11: substrate.

be 354.6 mm^3 using IPL, and then washed away the substrate in the lumps. The roots were put into 5-mL dosimeters, which were injected with known volumes of distilled water until the roots were all covered. Then the volumes at the liquid level were read. The root volumes were determined by subtracting the volume of distilled water from the liquid level volume as-read, and were found to be 336.4 mm^3. The root volumes determined from μCT segmented extraction method were 5.13% larger than those measured by the dosimeter method. The surfaces of root lumps were photographed using a digital camera. The distance at two random points on the lateral roots of a lump were measured on ImageJ (Rasband, 2011). Totally four segments of lateral roots were measured (Fig. 2A) and the average root length was 6.23 mm. On the 3D root images, the corresponding lateral root length was measured to be 6.02 mm on average, with error of 3.37% from the above method. Thus, the errors of the μCT segmented extraction method were very low.

To validate the precision of the pore segmented extraction method, we obtained CT images of root lump surface layer using μCT (Fig. 3A), segmented and extracted the pores (Fig. 3B). The lacunarity was measured to be 3.81%. The pore fractal dimension determined on the plug-in BoneJ of ImageJ (Michael *et al.*, 2010) was 1.153. Then the root lump surfaces as-scanned were photographed (Fig. 3C), and the surface pores of root lumps (Sun *et al.*, 2017a) could be clearly identified. The boundary lines of the pores were plotted on ImageJ and the lacunarity was 3.93%, which was larger than that estimated from μCT (3.15%), and the pore fractal dimension was 1.151, which was not significantly different from that determined from μCT. Thus, the errors of pores determined from the μCT segmented extraction method are very small.

Test and statistical methods

With pin shape, diameter and the initial pick-up angle as the test factors (Choi *et al.*, 2002; Han *et al.*, 2015), tests were conducted to optimize the pick-up parameters that reduced the destruction of root lumps. The tests were conducted in two steps. The gripper was designed as two-finger and four-pin (Fig. 4). The depth and contraction of a pick-up pin inserted into a root lump were 35 and 5 mm, respectively. Firstly, a 2.5 mm circular pick-up pin (Fig. 4A) was used to pick up a root lump at an initial pick-up angle θ of 21°; then the roots and pores were extracted from the lump and three-dimensionally reconstructed, aiming to find out the main causes of root lump destruction. Then the effects of pin shape, pin diameter and initial pick-up angle on root lump destruction were studied, aiming to find out the pick-up parameters when the root lump destruction was low. The pick-up conditions were: pick-up pin was circular or flat (Fig. 4), pin diameter *d* was 2, 2.5 or 3 mm, and the initial pick-up angle θ was 18°, 21° or 24°.

Since μCT can only scan stationary substances and to study the distributions of roots and pores during the pick-up process, we considered four states of each specimen: pick-up pin was not inserted into root lump (S1), pick-up pin was inserted into root lump (S2), pick-up pin was moved to the medium contraction (S3), and pick-up pin was moved to the maximum contraction (S4).

To study the root and pore distributions during the pick-up process, we divided each root lump into five equal zones vertically and six equal zones horizontally (Fig. 5) and defined the root distribution density as the ratio of root volume in each zone to the volume of root lump in this zone. Then the root volume, root distribution density, lacunarity, and pore fractal dimension in each zone were quantitatively analyzed. In each group, 10 samples were scanned, and totally there were 100 samples. The test data were stored on Excel. Single-

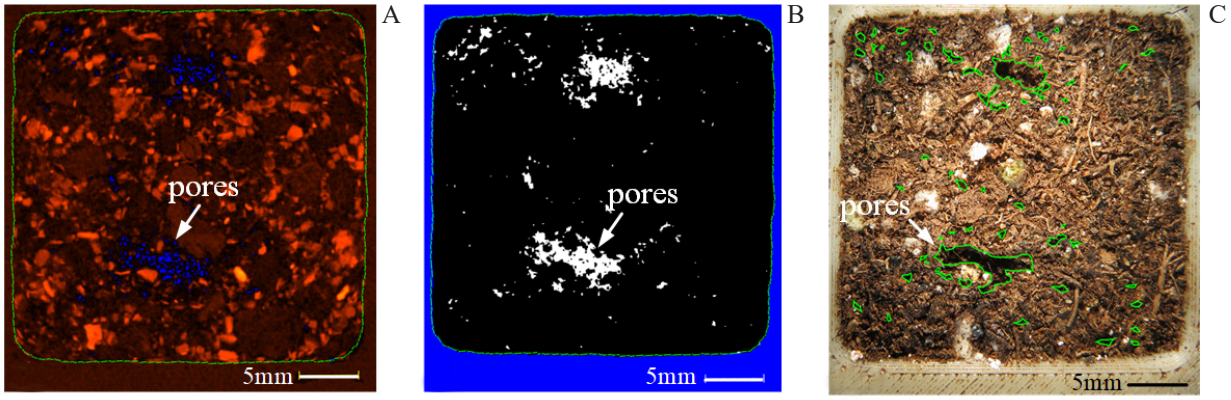

Figure 3. Root lump surface CT images from scanning (A), pore images from segmented extraction (B), and photographed root lump surface images (C).

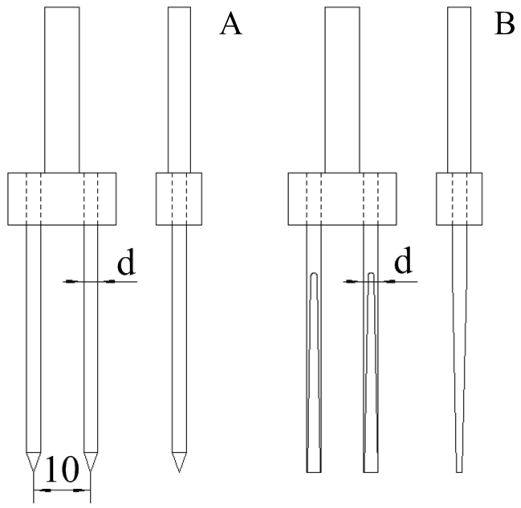

Figure 4. Structures of gripper with circular pick-up pin (A) and flat pick-up pin (B).

factor analysis of variance involving root volume, root distribution density, and lacunarity was conducted on SPSS 18.0. The mean values were compared via Tukey test, which required relatively small sample size.

Results and discussion

Root distributions during the pick-up process

Figure 6A shows the analytical values of vertical root volume V_{RV}. Clearly, the V_{RV} at each pick-up state first decreased and then increased. The statistics of V_{RV} are summarized in Table 1. When the pick-up pins contracted to state S4, the V_{RV} in zone V1 and V2 decreased, but V_{RV} in other zones rose. The change of V_{RV} varied insignificantly between -2.4 and 4.8 mm^3 ($p > 0.05$). Figure 6B shows the analytical values of horizontal root volume V_{RH}. Clearly, the V_{RH} at each pick-up state first increased and then decreased, which indicates a nearly symmetrical distribution. When the pick-up pins contracted to the largest displacement, V_{RH} decreased significantly in zones H1 and H6 by 4.2 and 4.1 mm^3, respectively ($p < 0.05$), but rose in other zones, V_{RH} increased insignificantly from 3.4 to 3.9 mm^3 ($p > 0.05$).

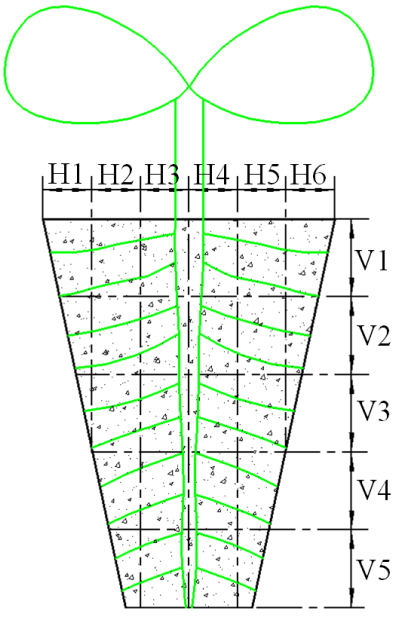

Figure 5. Schematic diagram of root lump division.

Figure 6A shows the analytical values of vertical root distribution density D_{RV}. Clearly, D_{RV} in zone V5 was significantly larger than at other zones. The statistics of D_{RV} are summarized in Table 1. When the pick-up pins contracted to the largest displacement, the D_{RV} in zone V1 and V2 decreased, but D_{RV} in other zones rose. The change of V_{RV} varied insignificantly between –0.05% and 0.14% ($p > 0.05$). Figure 6B shows the analytical values of horizontal root distribution density D_{RH}. Clearly, D_{RH} in zones H1 and H6 was significantly larger than at other zones. When the pick-up pins contracted to the largest displacement, the D_{RH} in zones H1 and H6 decreased significantly by 0.42% and 0.41%, respectively ($p < 0.05$), but D_{RH} in other zones rose insignificantly from 0.08% to 0.13% ($p > 0.05$).

Figure 7 shows the 3D root images. At each pick-up state, the roots formed similar spatial structures. Specifically, the lateral roots grew divergently from the main roots to the surroundings until contacting the pore walls. Then the lateral roots changed the growing direction and went on to grow along the pore walls and wind the root lumps. The distance between the outmost lateral roots at the same position under state S1 and state S4 was measured (Fig. 7A2, 7D2). Clearly, the horizontal distances between lateral roots were 24.57 and 23.19 mm, respectively, with a decrease of 1.38 mm, while the vertical distances were 24.86 and 25.21 mm, respectively, with an increment of 0.35 mm. Han *et al.* (2013) used a mechanical tester to compress cucumber root lumps and concluded that the root lumps were elastic-plastic bodied wrapped by roots and the root lumps reached the yield limit and plastically deformed when the compression force was 6.33 N. When a root lump was picked up by pins, shear stress and pressure stress existed inside the root lump. Under the action of the shear stress, the raising substrate shifted in the direction perpendicular to the pick-up pin contraction, bringing the roots to move outside the root lump. Under the pressure stress, the substrate moved in the root lump in parallel to the pick-up pin contraction (Karmakar *et al.*, 2007; Mojtaba *et al.*, 2013). When the pick-

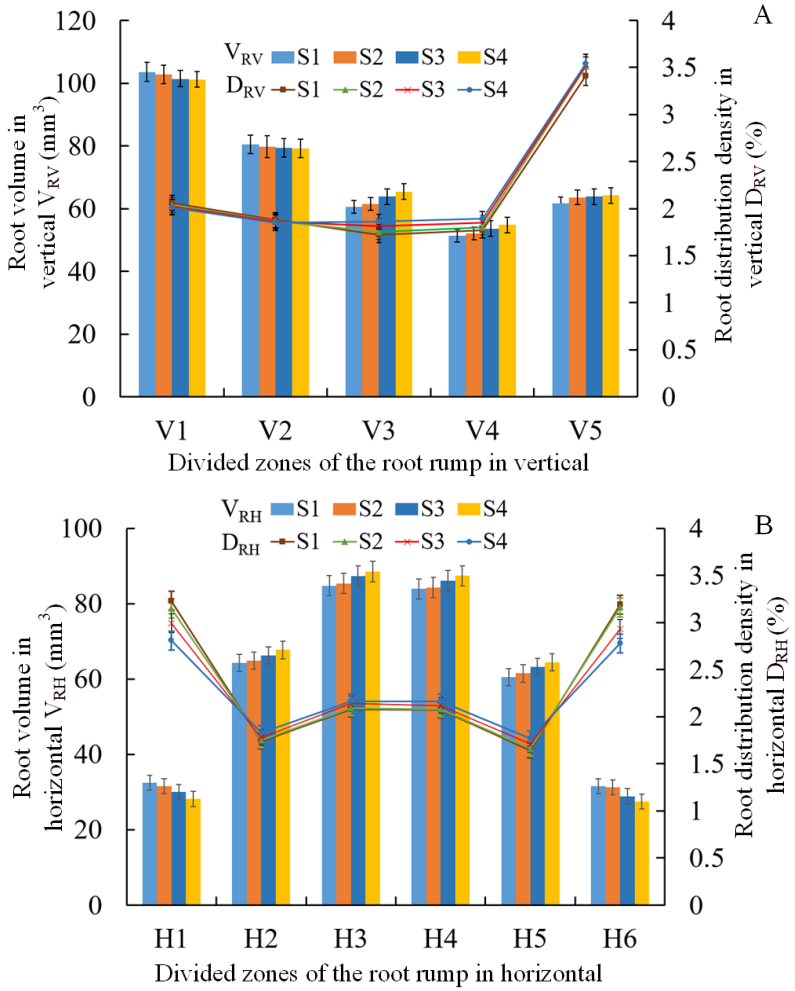

Figure 6. Analytical data of volumes and distribution density of the roots at the pick-up states at (A) vertical and (B) horizontal directions.

up pin contracted horizontally, the distance between the outmost lateral roots decreased horizontally and increased vertically (Fig. 7).

At the initial pick-up angle of 21º, when the pin diameter enlarged from 2 to 3 mm, the reduction of distance between the outmost lateral roots at the pin contraction direction rose from 1.27 to 1.56 mm, and the increment in the distance between the outmost lateral roots perpendicular to the pin contraction direction increased from 0.29 to 0.41 mm. At the pin diameter

Table 1. Statistics of root volumes and root distribution density.

No. of zone	Root volume (mm^3)				Change (mm^3)	Root distribution density (%)				Change (%)
	S1	S2	S3	S4		S1	S2	S3	S4	
V1	103.6^{a}	102.8^{a}	101.4^{a}	101.2^{a}	-2.4	2.06^{a}	2.04^{a}	2.02^{a}	2.01^{a}	-0.05
V2	80.5^{a}	79.8^{a}	79.4^{a}	79.2^{a}	-1.3	1.88^{a}	1.87^{a}	1.86^{a}	1.85^{a}	-0.03
V3	60.6^{a}	61.5^{a}	63.8^{a}	65.4^{a}	4.8	1.72^{a}	1.75^{a}	1.81^{a}	1.86^{a}	0.14
V4	51.4^{a}	52.1^{a}	53.6^{a}	54.8^{a}	3.4	1.77^{a}	1.80^{a}	1.85^{a}	1.89^{a}	0.12
V5	61.7^{a}	63.6^{a}	63.8^{a}	64.2^{a}	2.5	3.41^{a}	3.51^{a}	3.52^{a}	3.54^{a}	0.13
H1	32.4^{a}	31.6^{a}	30.1^{ab}	28.2^{b}	-4.2	3.23^{a}	3.15^{a}	2.99^{ab}	2.81^{b}	-0.42
H2	64.3^{a}	64.9^{a}	66.3^{a}	67.7^{a}	3.4	1.74^{a}	1.75^{a}	1.78^{a}	1.83^{a}	0.09
H3	84.8^{a}	85.4^{a}	87.3^{a}	88.5^{a}	3.7	2.08^{a}	2.09^{a}	2.14^{a}	2.16^{a}	0.08
H4	83.9^{a}	84.3^{a}	86.1^{a}	87.4^{a}	3.5	2.07^{a}	2.08^{a}	2.12^{a}	2.16^{a}	0.09
H5	60.5^{a}	61.5^{a}	63.2^{a}	64.4^{a}	3.9	1.64^{a}	1.66^{a}	1.71^{a}	1.77^{a}	0.13
H6	31.6^{a}	31.3^{a}	28.9^{ab}	27.5^{b}	-4.1	3.19^{a}	3.16^{a}	2.93^{ab}	2.78^{b}	-0.41

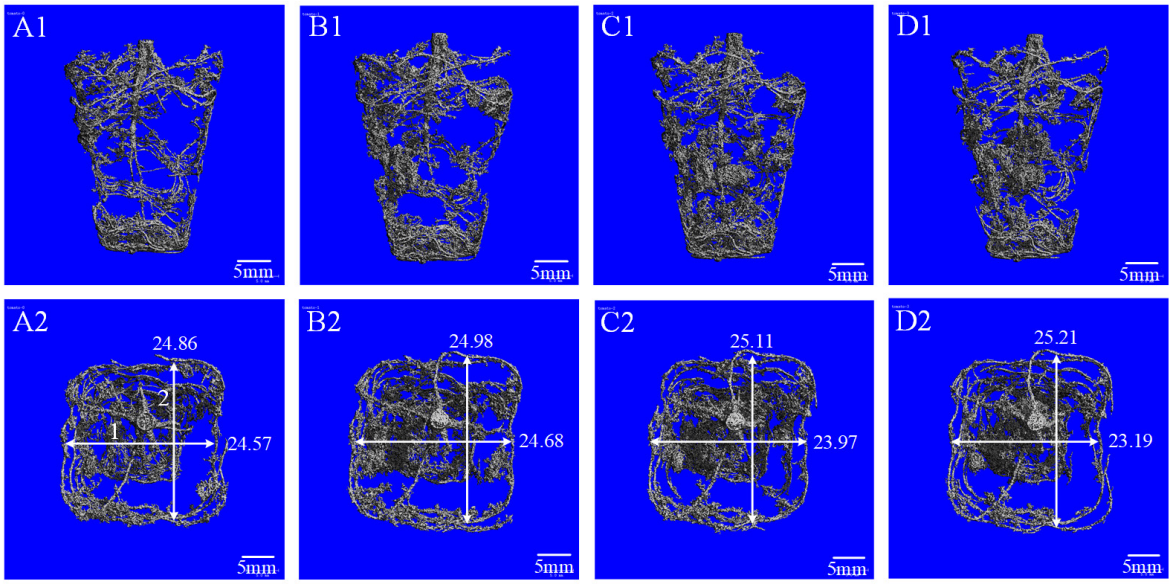

Figure 7. Front view (A1, B1, C1, D1) and top view (A2, B2, C2, D2) 3D visualized images of roots at states S1 (A1, A2), S2 (B1, B2), S3 (C1, C2) and S4 (D1, D2). Distance between outmost lateral roots at (1) horizontal and (2) vertical directions.

of 2.5 mm, when the initial pick-up angle enlarged from 18º to 24 º, the reduction of distance between the outmost lateral roots at the pin contraction direction decreased from 1.61 to 1.29 mm, and the increment in the distance between the outmost lateral roots perpendicular to the pin contraction direction declined from 0.43 to 0.31 mm. Clearly, the increments in the distance between the outmost lateral roots were very small, which was because the hole walls restricted the outward expansion of the root lumps. During the pick-up process, though the outmost lateral roots shifted, the spatial distribution of roots did not change significantly, as the roots always wrapped the raising substrate and thereby prevented the root lumps from loosening (Shaw, 1993; Han *et al.*, 2015).

Pore distributions on CT images during the pick-up process

The root lumps were scanned to generate 800 CT images, from which one image every 180 images was selected. Totally, four images were selected, in which the first to third images all were passed through by pick-up pins (Fig. 8).

From the first to the third images, the pores at state S1 were scattered; as the contracting displacement of the pick-up pins was intensified, more new pores were formed and connected to form larger pores (Keyes *et al.*, 2013). However, on the fourth image, the number of pores decreased when the contracting displacement of pick-up pins was enhanced. Table 2 shows the pore areas on the CT images at different states. The pore areas were gradually enlarged on the first to third images, but were reduced on the fourth image, while the changes of pore areas varied significantly between -4.7 and 8.7 mm^2 on the four images ($p < 0.05$). The areas of largest pores on the CT images were statistically analyzed on Image J (Table 2). When the pick-up pins contracted to state S4, the pore areas on images 1 to 3 increased by 1.76, 1.22 and 0.71 mm^2, respectively, but that in image 4 decreased by 0.49 mm^2; the largest pore area varied very significantly among the four images ($p < 0.05$). Clearly, the newly-formed pores mainly appeared on the CT images in contact with pick-up pins, but the pore areas decreased in the images without contact with the pins.

Pore distributions in 3D space during the pick-up process

Figure 9A shows the analytical values of vertical lacunarity D_{PV}. Clearly, the D_{PV} at each pick-up state changed differently. The statistics of lacunarity at different states were summarized in Table 3. When the pick-up pins contracted to the largest displacement, the changes of D_{PV} in zones V1 to V5 varied significantly between -4.09% and 4.74% ($p < 0.05$). Figure 9B shows the analytical values of horizontal lacunarity D_{PH}. Clearly, the V_{PH} was almost symmetrically distributed at each pick-up state. When the pick-up pins contracted to state S4, the changes of D_{PH} in zones H1 to H6 varied significantly between 0.32% and 5.94% ($p < 0.05$).

Figure 9A shows the analytical data of vertical pore fractal dimension F_{PV} and Table 3 lists the statistical data. During the pick-up process, the F_{PV} first decreased and then increased in all zones from V1 to V4, but F_{PV}

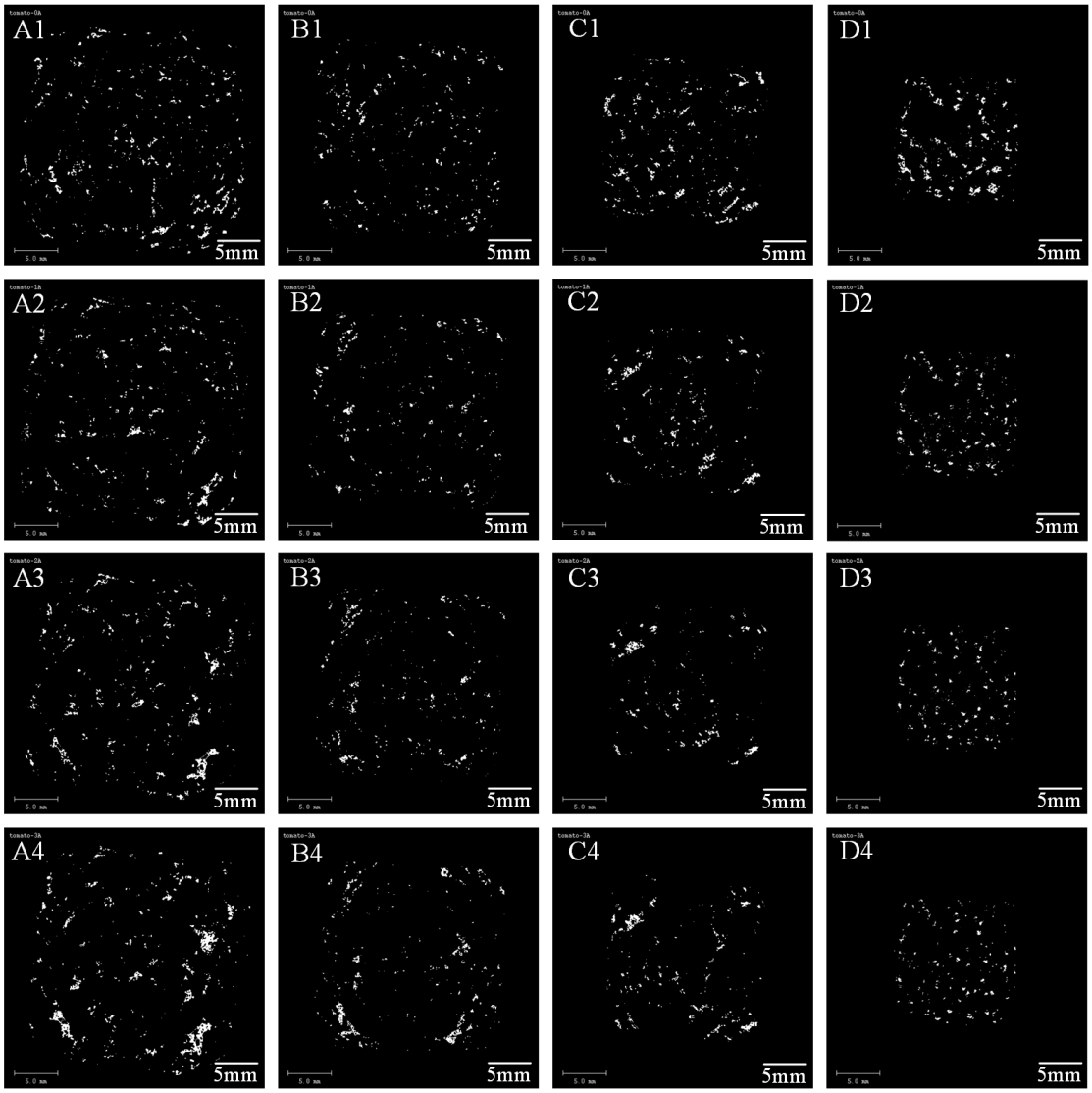

Figure 8. CT images of pores at states S1 (A1, B1, C1, D1), S2 (A2, B2, C2, D2), S3 (A3, B3, C3, D3) and S4 (A4, B4, C4, D4) on images 1 (A1, A2, A3, A4), 2 (B1, B2, B3, B4), 3 (C1, C2, C3, C4) and 4 (D1, D2, D3, D4).

in zone V5 declined. Figure 9B displays the analytical values of horizontal pore fractal dimension F_{PH}. Clearly, the F_{PH} first declined and then increased in all zones, and the F_{PH} was almost symmetrically distributed in all the pick-up states.

Figure 10 shows the spatial pore distributions at different pick-up states. At state S1, the pores accumulated at the top and bottom of the root lumps, but the pores at other positions were scattered. The permeable top of root lumps facilitated water evaporation, while the roots at the bottom promoted the migration of the raising substrate during the growing period (Fig. 7). These two situations both led to pore aggregation. At the S2 state, the pick-up pins inserted

Table 2. Pore areas and areas of largest pores on CT images at different pick-up states.

No. of pore image	Pore area (mm^2)				Change (mm^2)	Area of largest pore (mm^2)				Change (mm^2)
	S1	S2	S3	S4		S1	S2	S3	S4	
1	39.1^{d}	42.3^{c}	45.7^{b}	47.8^{a}	8.7	0.59^{d}	1.02^{c}	1.73^{b}	2.35^{a}	1.76
2	22.0^{d}	23.9^{c}	26.3^{b}	28.6^{a}	6.6	0.31^{c}	0.87^{b}	1.13^{b}	1.53^{a}	1.22
3	19.4^{d}	21.2^{c}	23.5^{b}	25.6^{a}	6.2	0.54^{c}	0.82^{b}	1.06^{a}	1.25^{a}	0.71
4	20.3^{a}	17.5^{b}	16.3^{c}	15.6^{c}	-4.7	0.65^{a}	0.29^{b}	0.21^{b}	0.16^{b}	-0.49

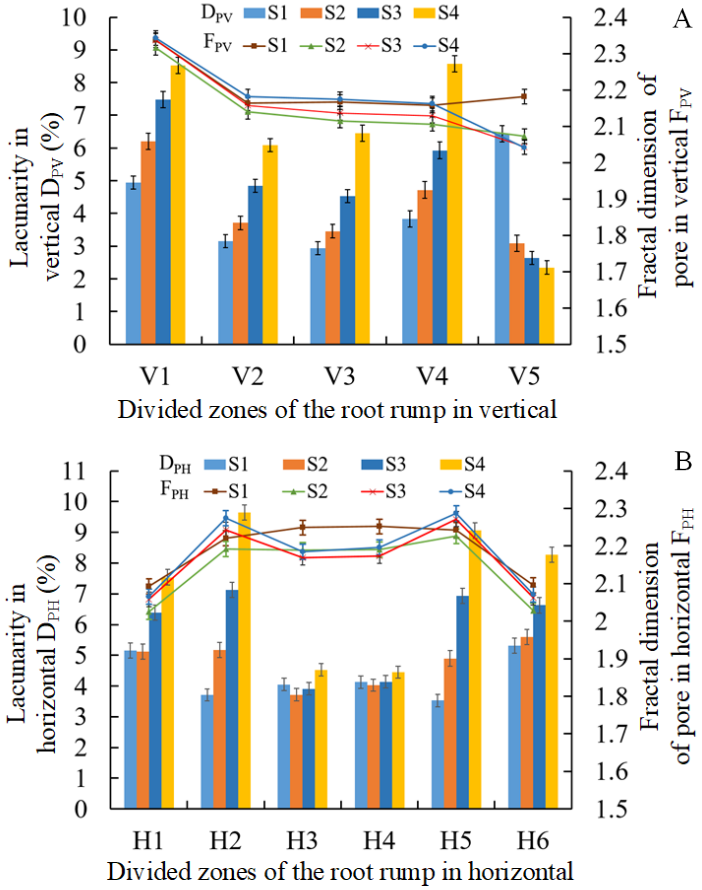

Figure 9. Analytical data of lacunarity and pore fractal dimension at pick-up states at (A) vertical and (B) horizontal directions.

into the root lumps urged the migration of the raising substrate, while cracks and newly-formed pores gathered around the pick-up pins; under the action of shear stress, new pores also appeared in between the pick-up pins (Espinoza *et al.*, 2016; Sun *et al.*, 2017b). Under the pressure stress, the raising substrates far from the pick-up pins mutually extruded, leading to pore closure, and especially when the pick-up pins did not reach the bottom of root lumps, the number of pores significantly decreased (Karmakar *et al.*, 2007; Mojtaba *et al.*, 2014). From state S3 to state S4, the pin contraction and migration directly avulsed the root lumps, and the cracks outside the pick-up pins started to expand and generated more new pores. In some areas, the cracks

Table 3. Statistics of lacunarity and pore fractal dimension.

No. of zone	Lacunarity (%)				Change (%)	Pore fractal dimension			
	S1	S2	S3	S4		S1	S2	S3	S4
V1	4.94^{d}	6.21^{c}	7.48^{b}	8.53^{a}	3.59	2.336	2.315	2.337	2.342
V2	3.15^{d}	3.71^{c}	4.84^{b}	6.09^{a}	2.94	2.164	2.139	2.157	2.182
V3	2.94^{d}	3.46^{c}	4.53^{b}	6.45^{a}	3.51	2.167	2.115	2.136	2.174
V4	3.83^{d}	4.72^{c}	5.93^{b}	8.57^{a}	4.74	2.157	2.106	2.129	2.162
V5	6.44 ^{a}	3.09^{b}	2.64^{bc}	2.35^{c}	-4.09	2.181	2.072	2.043	2.041
H1	5.16^{c}	5.12^{c}	6.39^{b}	7.54^{a}	2.38	2.093	2.025	2.058	2.065
H2	3.71^{d}	5.17^{c}	7.13^{b}	9.65^{a}	5.94	2.221	2.192	2.243	2.274
H3	4.05 ^{b}	3.72^{b}	3.91^{b}	4.53^{a}	0.48	2.249	2.189	2.169	2.185
H4	4.13^{ab}	4.03^{b}	4.14^{a}	4.45^{a}	0.32	2.252	2.191	2.174	2.196
H5	3.53^{d}	4.90^{c}	6.93^{b}	9.06^{a}	5.53	2.243	2.226	2.272	2.287
H6	5.31^{c}	5.60^{c}	6.63^{b}	8.27^{a}	2.96	2.095	2.028	2.063	2.071

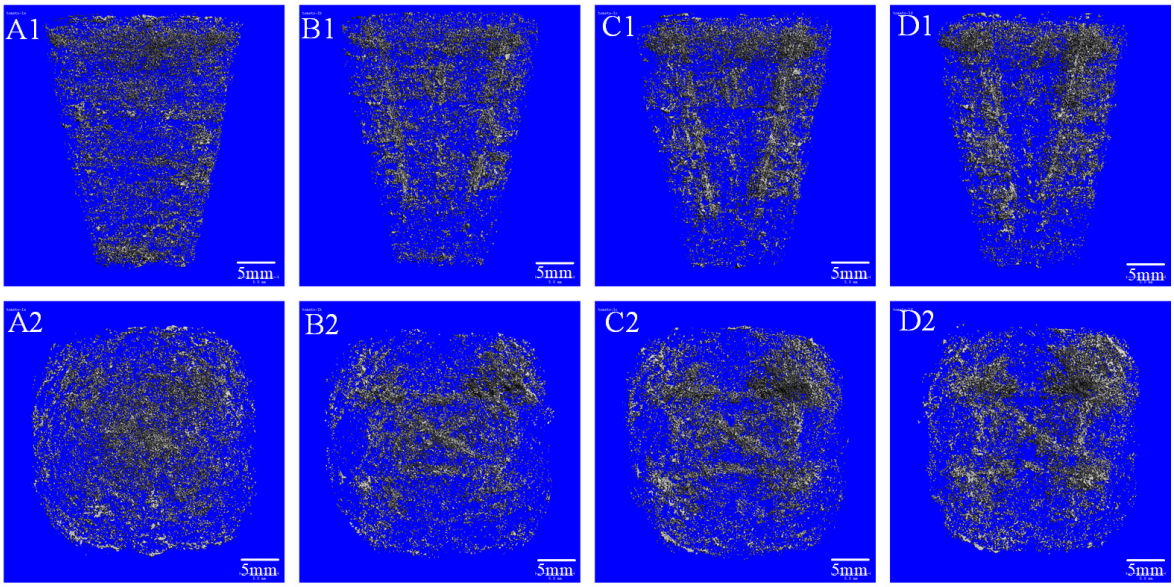

Figure 10. Front view (A1, B1, C1, D1) and top view (A2, B2, C2, D2) 3D visualized images of pores at states S1 (A1, A2), S2 (B1, B2), S3 (C1, C2) and S4 (D1, D2).

already expanded to the outmost end of the root lumps. Under the pressure stress, the pores in between the pick-up pins were closed, and at the exterior areas far from the pick-up pins, the pores were not obviously changed after the pick-up pins inserted into the root lumps.

In the zones V1 to V4, H2 and H5 which directly contacted the pick-up pins, the lacunarity gradually increased, but the fractal dimensions firstly decreased and then rose, and the fractal dimensions at state S4 surpassed those at state S1 (Fig. 9). At state S2, the pores and cracks were distributed nonuniformly in all zones and appeared more around the pins, but the number of pores far from the pins declined. The formation of cracks enlarged the lacunarity, while the local aggregation of cracks and the decreasing number of pores distant from the pins together led to a reduction of fractal dimensions (Annette & Martin, 2005; Lars *et al.*, 2012). At states S3 and S4, the expanding cracks and the new pores spread to large space in all zones, so that the lacunarity and fractal dimensions increased in zones V1 to V4, H2 and H5 (Zhao *et al.*, 2017). At state S2, in zones H1, H3, H4 and H6 that did not contact with the pins, the pores were closed and thus the lacunarity and fractal dimensions decreased. When the pick-up pins contracted and moved to state S4, the cracks and pores around the pins already expanded to zones H1 and H6, while the top of the pins moved to H3 and H4. The numbers and distrubtive areas of both cracks and pores all increased in the above four zones, leading to the increase of lacunarity and fractal dimensions to varying degrees. When the water contents of root lumps increase, the small pores in the root lumps are filled with water, which prevented the new pore generation and crack expansion. However, too high water contents would weaken the anti-deformation ability of root lumps, and consequently, the root lumps would fall off when the grippers pick up root lumps. As reported, when the water contents of root lumps were 50%-65%, the anti-destruction ability and pick-up success rate of root lumps were the optimal (Mao *et al.*, 2014; Han *et al.*, 2015).

The pick-up pin to pick up a root lump should overcome the adhesion between the root lump and the hole walls, which leads to stress concentration in zone V4 (where cracks are enlarged) and in zone V5 (where the number of pores decreases) and finally breaks the root lump. To diminish the occurrence of fracture, workers should insert the pick-up pins into the root lumps as deep as possible (Tong *et al.*, 2013; Jiang *et al.*, 2017). In zones H2 and H5 where the pick-up pins contracted, the lacunarity increased the most largely. If the pores and cracks in these two zones expanded to outside the root lumps or connected to form fracture surfaces, the raising substrate and the root lumps would be partially separated, leading to the destruction of root lumps. The destruction of root lumps can be deminished by optimizing the pin structures and pick-up parameters (Yang *et al.*, 1991; Ryu *et al.*, 2001; Jiang *et al.*, 2017).

Determination of evaluation index for root lump destruction

The distributions of roots and pores during the pick-up process show the pore aggregation and crack formation were the main causes of root lump destruction.

V4 was called the fracturable zone, while H2 and H5 were the breakable zones. Root lump destruction can be evaluated using the lacunarity of these zones at state S4. During the pick-up of root lumps, the root lumps would be destroyed when the cracks expanded to a certain degree. The cracks in Figure 11 spread to the two ends of the root lumps, where destruction was observed. A rectangular frame was plotted with the longest distance of cracks as the diagonal line. Then the lacunarity of 60 consecutive CT graphs within this rectangle was statistically analyzed to be 16.8%, which was considered as the destruction index. It was thought that the fracturable zone and breakable zone in which the lacunarity reached this index would be destroyed.

Optimization of pick-up parameters

When the pin diameter was 2 mm and the initial pick-up angle was 24º, the lacunarity in the fracturable zone (D_{PD}) and the lacunarity at the breakable zone (D_{PS}) for the circular pick-up pins both minimized. The D_{PD} and D_{PS} of flat pick-up pins both maximized when the pin diameter was 3 mm and the initial pick-up angle was 18º. All tested factors significantly affected both D_{PD} and D_{PS} ($p < 0.05$) (Fig. 12).

The D_{PD} and D_{PS} of both circular and flat pins rose with the increase of pin diameter (Fig. 12A). At the pin diameter of 2, 2.5 and 3 mm, the D_{PD} of the circular pins was 7.1%, 8.5% and 9.8%, respectively, and the D_{PS} was 8.1%, 9.4% and 11.3%, respectively, while the D_{PD} of flat pins was 8.2%, 10.6% and 12.4%, respectively, and the D_{PS} was 9.0%, 10.8% and 12.9%, respectively. Clearly, the D_{PS} of the flat pins maximized at the pin diameter of 3 mm, which was 3.9% smaller than the destruction index, so the possibility of root lump breakage was higher. At the pin diameter of 2 mm, the D_{PS} and D_{PD} were both more than 7.8% smaller than the destruction index for both the circular pins and the flat pins, so the possibility of lump destruction was lower. Thus, to reduce the destruction of root lumps, the pick-up pin diameter should be decreased. However, to get enough clamping force in the thin pins and to overcome the adhesion between root lumps and hole walls, the shrinkage of pins should be increased (Choi *et al.*, 2002; Tong *et al.*, 2014), which would promote crack expansion. Moreover, thin pins would be bent due to the insufficient rigidity, which was unfavorable for the pick-up of seedlings. Thus, the destruction to root lumps did not decrease with the reduction of pin thickness. For multi-pin grippers, the pins in diameter of 2 mm already had excellent pick-up performance (Han *et al.*, 2015).

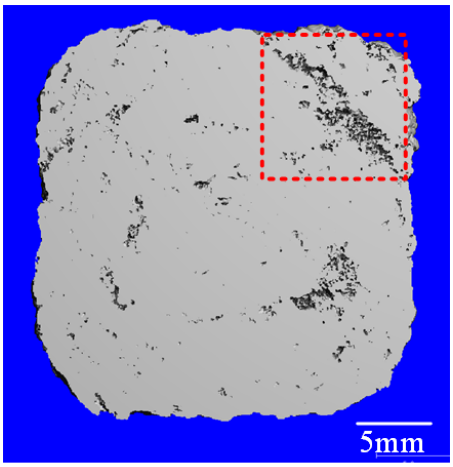

Figure 11. Sections of root lumps containing cracks.

As the initial pick-up angle was enlarged, the D_{PD} and D_{PS} both gradually declined for both the circular and flat pins (Fig. 12B). At the initial pick-up angle of 18º, 21º and 24º, the D_{PD} of the circular pins was 9.9%, 8.5% and 7.4%, respectively, and the D_{PS} was 11.7%, 9.4% and 8.5%, respectively, while the D_{PD} of flat pins was 13.6%, 10.6% and 9.3%, respectively, and the D_{PS} was 13.9%, 10.8% and 9.7%, respectively. Clearly, the D_{PD} and D_{PS} of the flat pins both maximized at the initial pick-up angle of 18º, which were 3.2% and 2.9% smaller than the destruction index, so the root lumps were more easily destroyed. At the initial pick-up angle of 24º, the D_{PD} and D_{PS} were both over 7.1% smaller than the destruction index for both the circular pins and the flat pins, so the possibility of root lump destruction was lower. The destruction of root lumps can be eliminated by increasing the initial pick-up angle. However, when the initial pick-up angle surpassed the hole wall included angle and to acquire certain quantity of contraction, the insertion depth of pick-up pins should be shortened, which would reduce the clamping force and move the fracturable area upwards, and the destruction of root lumps would be more severe. One efficient solution is to change the direction of pin contraction, so that the pins would contract from the diagonal line of the root lump sections to the center, which would enlarge the initial pick-up angle and increase the distance and clamping force between the pins (Han *et al.*, 2015; Jiang *et al.*, 2017).

At the same pick-up conditions, the D_{PD} and D_{PS} of flat pins always surpassed those of circular pins (Fig. 12). As for the reasons, the circular pins were in round face contact, and the raising substrate would slip bilaterally during the pin contraction, which would weaken the shearing and compression on the substrate caused by the pins. On the contrary, the flat pins were in plane contact with the substrate, which would more promote the migration of the substrate, and the new

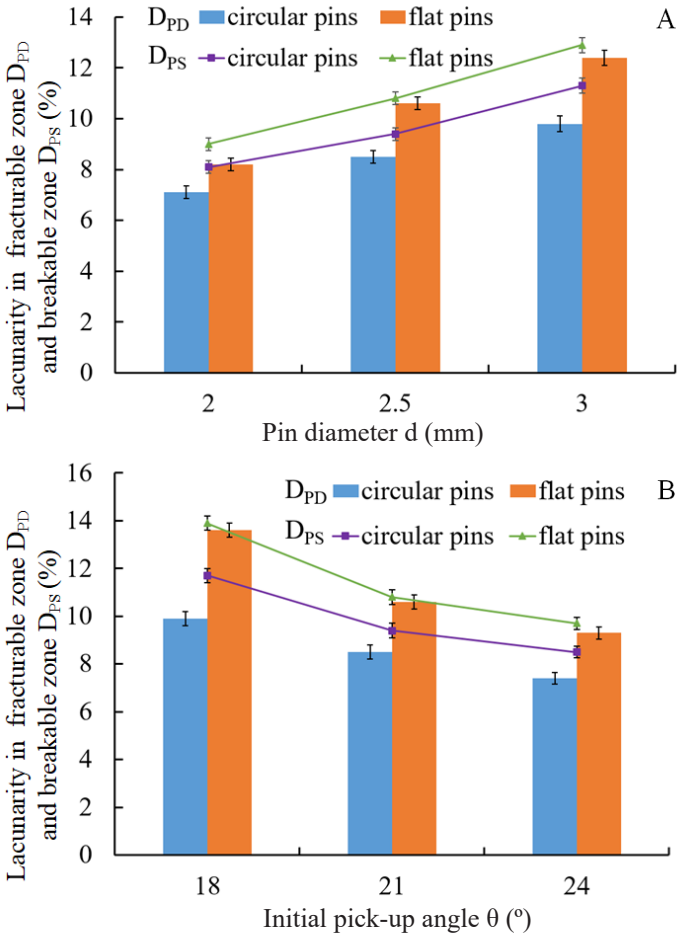

Figure 12. Analytical data of lacunarity in the fracturable zone and breakable zone when pin diameter (A) and initial pick-up angle (B) changed.

pore aggregation and crack formation in the root lumps would be more significant (Karmakar *et al.*, 2007; Mojtaba *et al.*, 2013). The destruction of root lumps could be diminished by optimizing the sectional shape of pick-up pins, such as ellipse and semi-circle.

Generally, there is a group of optimal pick-up parameters that could reduce the pore aggregation and crack expansion in the root lumps. The possibility of root lump destruction over the circular pins minimized when the pin diameter was 2 mm and the initial pick-up angle was 24º.

Validation of pick-up parameters

To validate the reasonableness of pick-up parameters as-selected, we used the automatic transplant structure to test seedling pick-up (Fig. 13A). When this structure worked, the feeding tray device and the gripper moved synchronously, which ensured the tomato plug seedlings were taken out of the trays one-by-one. The swing of the gripper was controlled by a circular cylinder, so the tomato plug seedlings were taken out of the trays and devoted into the cast seedling cups. The gripper was a 2-finger 4-pin structure (Fig. 13B), and the contraction and stretching of the pick-up pins were controlled by a squared cylinder. During the trials, the seedling pick-up rate was 45 plants/min.

Trials were conducted in accordance with Table 7. In each group of trials involving 512 plants, either pin diameter *d* or initial pick-up angle θ was altered. When the mass loss exceeded 25%, the root lump was considered as severely damaged (Choi *et al.*, 2002).

The root lump destruction rate R was calculated as follows:

$$R = \frac{N_2}{N_1} \times 100\%$$

where N_1 is the number of tomato plug seedlings in each group; N_2 is the number of tomato plug seedlings with root lump mass loss > 25%.

When the pin diameter *d* was 2 mm and the initial pick-up angle θ increased from 18° to 24°, the root lump destruction rates over circular pins and flat pins decreased from 12.62% to 6.63% and from 14.35% to

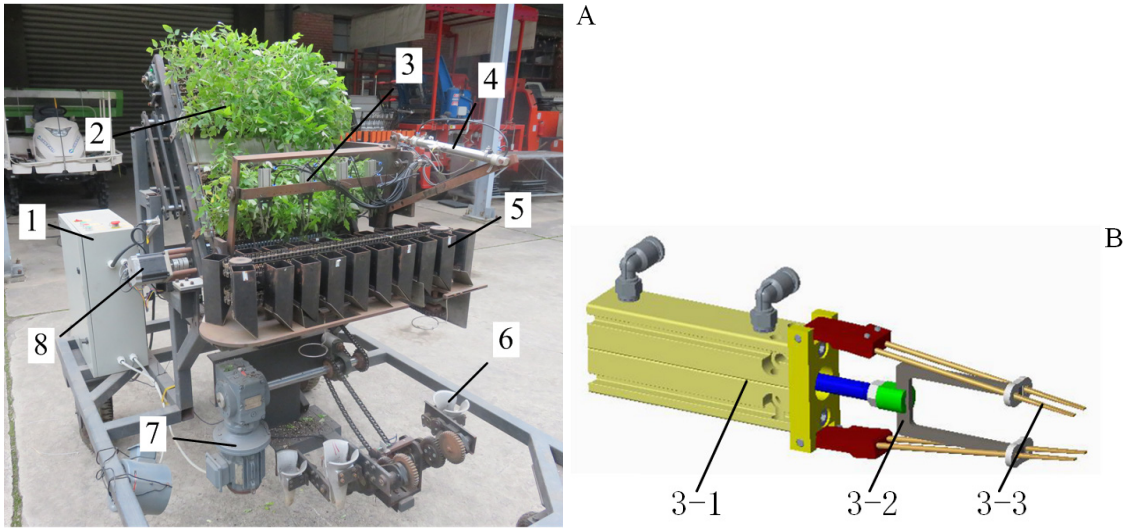

Figure 13. Automatic transplant structure (A) and gripper (B). 1. control system; 2. feed tray device; 3. gripper; 4. circular cylinder; 5. cast seedling cup; 6. planter; 7. driving generator of planter; 8. driving generator of feeding tray; 3-1. squared cylinder; 3-2. control pole; 3-3. pick-up pin.

7.87%, respectively (Table 4). When θ was 24° and *d* increased from 2 to 3 mm, the root lump destruction rates over circular pins and flat pins increased from 6.63% to 10.32% and from 7.87% to 12.16%, respectively. The root lump destruction rates decreased with the increase of θ and rose with the increase of *d* irrespective of pin shape. At the same pick-up conditions, the root lump destruction rates with the use of circular pins were smaller than over flat pins. The root lump destruction rate over the 2-mm-diameter circular pins at the initial pick-up angle 24° was the smallest. The findings of seedling pick-up trials are consistent with the results of pick-up parameter optimization.

In conclusion, the tomato root lumps were scanned by X-ray microcomputed tomography, and thereby the roots and pores were extracted and three-dimensionally reconstructed. During the pick-up process, the roots always wrapped the raising substrate and prevented the root lumps from loosening. The main causes for the root lump fracturing and breakage were the pore aggregation and the crack formation respectively at the apex & circumference of the pick-up pins. The lacunarity in the these two zones can be used to judge the destruction degrees of root lumps, and it was found the lacunarity in the fracturable zones and the breakable zones can be decreased by decreasing the pin diameter (2, 2.5, 3 mm) and enlarging the initial pick-up angle (18º, 21º, 24º). Under the same pin contraction quantity, the destruction to root lumps by circular pick-up pins was less severe compared with flat pins and was minimized when the pin diameter was 2 mm and the initial pick-up angle was 24º. During pick-up experiments with the auto-transplant structures, the destruction to root lumps under this combination of pick-up parameters minimized to 6.63%. The optimized pick-up parameters can be used to guide pick-up claw design and to improve the working performance of automatic transplanters.

Table 4. Test parameters and results R (%).

No. of test	Pin shape	*d* (mm)	θ (°)	R (%)
1	Circular	2	18	12.62
2	Circular	2	21	9.54
3	Circular	2	24	6.63
4	Circular	2.5	24	8.32
5	Circular	3	24	10.32
6	Flat	2	18	14.35
7	Flat	2	21	10.96
8	Flat	2	24	7.87
9	Flat	2.5	24	9.71
10	Flat	3	24	12.16

d: pin diameter. θ: Initial pick-up angle. R: destroyed rate of root lump.

References

Annette D, Martin T, 2005. The relationship between fractal properties of solid matrix and pore space in porous media. Geoderma 129: 279-290. https://doi.org/10.1016/j.geoderma.2005.01.003

Choi JM, Lee C, Chun JP, 2012. Optimization of substrate formulation and mineral nutrition during the production of vegetable seedling grafts. Hortic Environ Biotechnol 53 (3): 212-221. https://doi.org/10.1007/s13580-012-0108-1

Choi WC, Kim DC, Ryu IH, Kim KU, 2002. Development of a seedling pick-up device for vegetable transplanters. T ASAE 45 (1): 13-19. https://doi.org/10.13031/2013.7864

Espinoza DN, Shovkun I, Makni O, Lenoir N, 2016. Natural and induced fractures in coal cores imaged through X-ray computed microtomography–Impact on desorption time. Int J Coal Geol 5: 165-175. https://doi.org/10.1016/j.coal.2015.12.012

Fukushima T, Sato K, Saito H, Nakamura S, Ohi T, 2012. Bending characteristics of cabbage plug seedlings on working precision of automatic transplanter. Jap J Farm Work Res 5 (4): 133-139. https://doi.org/10.1016/S1881-8366(12)80009-7

Han LH, Mao HP, Hu JP, Miao XH, Tian KP, Yang XY, 2013. Experiment on mechanical property of seedling pot for automatic transplanter. T CSAE 29 (2): 24-29.

Han LH, Mao HP, Hu JP, Tian KP, 2015. Development of a doorframe-typed swinging seedling pick-up device for automatic field transplantation. Span J Agric Res 13 (2): 1-14. https://doi.org/10.5424/sjar/2015132-6992

Hu JP, Yan XY, Ma J, Qi CH, Francis K, Mao HP, 2014. Dimensional synthesis and kinematics simulation of a high-speed plug seedling transplanting robot. Comput Electron Agr 107: 64-72. https://doi.org/10.1016/j.compag.2014.06.004

Jiang ZH, Hu Y, Jiang HY, Tong JH, 2017. Design and force analysis of end-effector for plug seedling transplanter. Plos One 12 (7): 1-15. https://doi.org/10.1371/journal.pone.0180229

Jin X, Du XW, Ji JT, Wang SG, Dong X, Du MM, 2015. Mechanical property experiment of plug seeding with pots gripping-picking. Int Agr Eng J 24 (4): 24-33.

Kalender WA, Hebel R, Ebersberger J, 1987. Ion of CT artifacts caused by metallic implants. Radiology 164 (2): 576-577. https://doi.org/10.1148/radiology.164.2.3602406

Karmakar S, Kushwaha RL, Lague C, 2007. Numerical modelling of stress and pressure dietribution on a flat tillage tool using computational fluid dynamics. Biosyst Eng 97: 407-414. https://doi.org/10.1016/j.biosystemseng.2007.02.008

Keyes SD, Boardman RP, Marchant A, Roose T, Sinclai RI, 2013. A robust approach for determination of the macro-porous volume fraction of soils with X-ray computed tomography and an image processing protocol. Eur J Soil Sci 64: 297-307. https://doi.org/10.1111/ejss.12019

Kumar GVP, Raheman H, 2008. Vegetable transplanters for use in developing contries-a review. Int J Veg Sci 14 (3): 232-255. https://doi.org/10.1080/19315260802164921

Kumar GVP, Raheman H, 2010. Volume of vermicompost-based potting mix for vegetable transplants determined using fuzzy biomass growth index. Int J Veg Sci 16: 335-350. https://doi.org/10.1080/19315260.2010.482951

Kumi F, Mao H, Li Q, Luhua H, 2016. Assessment of tomato seedling substrate-root quality using X-ray computed tomography and scanning electron microscopy. Amn Soc Agr Biol Eng 32 (3): 1-11.

Lars JM, Richard JH, Bill D, 2012. Soil pore characteristics assessed form X-ray micro-CT derived images and correlation to soil friability. Geoderma 181-182: 22-29. https://doi.org/10.1016/j.geoderma.2012.02.024

Mao H, Han L, Hu J, Kumi F, 2014. Development of a pincette-type pick-up device for automatic transplanting of greenhouse seedlings. Appl Eng Agr 30 (4): 547-556. https://doi.org/10.13031/aea.30.10550

Michael D, Michal Mk, Ignacio AC, Fabrice PC, Robert PD, Jonathan SJ, Benjamin S, John RH, Sandra JS, 2010. BoneJ: Free and extensible bone image analysis in ImageJ. Bone 47: 1076-1079. https://doi.org/10.1016/j.bone.2010.08.023

Mojtaba NB, Reza A, Abbas H, Ahmad S, Alireza K, Mehari ZT, Thomas K, 2013. 3D finite element simulation of a single-tip horizontal penetrometer-soil interaction. Part I: Development of the model and evaluation of the model parameters. Soil Till Res 134: 153-162. https://doi.org/10.1016/j.still.2013.08.002

Mojtaba NB, Reza A, Abbas H, Ahmad S, Alireza K, Mehari ZT, Thomas K, 2014. 3D finite element simulation of a single-tip horizontal penetrometer-soil interaction. Part II: Soil bin verification of the model in a clay-loam soil. Soil Till Res 144: 211-219. https://doi.org/10.1016/j.still.2014.03.008

Mooney SJ, Pridmore TP, Helliwell J, Bennett MJ, 2012. Developing X-ray computed tomography to non-invasively image 3-D root systems architecture in soil. Plant Soil 352: 1-22. https://doi.org/10.1007/s11104-011-1039-9

Nandede BM, Raheman H, Kumar GVP, 2014. Standardization of potting mix and pot volume for the production of vegetable seedlings in paper pot. J Plant Nutr 37 (8): 1214-1226. https://doi.org/10.1080/01904167.2014.881867

Rasband W, 2011. ImageJ. National Institute of Health. http://imagej.nih.gov/ij/

Richard JF, Christopher NG, Matthew T, Michelle W, Ann M, Iain MY, 2012. Non-destructive quantification of cereal roots in soil using high-resolution X-ray tomography. J Exp Bot 63 (7): 2503-2511. https://doi.org/10.1093/jxb/err421

Roberson DD, Yuan J, Wang G, 1997. Total hip prosthesis metal-artifact suppression using iterative deblurring reconstruction. J Comput Assist Tomogr 21 (2): 293-298. https://doi.org/10.1097/00004728-199703000-00024

Ryu KH, Kim G, Han JS, 2001. Development of a robotic transplanter for bedding plants. J Agric Eng Res 78 (2): 141-146. https://doi.org/10.1006/jaer.2000.0656

Saoirse RT, Colin RB, Jeremy AR, Sacha JM, 2013. Exploring the interacting effect of soil texture and bulk distribution density on root system development in tomato (Solanum lycopersicum L). Environ Exp Bot 91: 38-47. https://doi.org/10.1016/j.envexpbot.2013.03.003

Shaw LN, 1993. Changes needed to facilitate automatic field transplanting. Hort Tech 3 (4): 418-420. https://doi.org/10.21273/HORTTECH.3.4.418

Stefan M, Craig S, Darren MW, Malcolm JB, Sacha JM, Tony PP, 2015. On the evaluation of methods for the recovery of plant root systems from X-ray computed tomography images. Funct Plant Biol 42: 460-470. https://doi.org/10.1071/FP14071

Sun CD, Ding WM, Zhou LF, Qiu W, Gu JB, 2017a. Design and application of a system for droplet-size measurement in the field based on micro-distance imaging technology. Crop Prot 96: 228-236. https://doi.org/10.1016/j.cropro.2017.02.013

Sun W, Hou KP, Yang ZQ, Wen YM, 2017b. X-ray CT three-dimensional reconstruction and discrete element analysis of the cement paste backfill pore structure under uniaxial compression. Construct Build Mater 138: 69-79. https://doi.org/10.1016/j.conbuildmat.2017.01.088

Tong JH, Li JB, Jiang HY, 2013. Machine vision techniques for the evaluation of seedling quality based on leaf area. Biosyst Eng 115 (3): 369-379. https://doi.org/10.1016/j.biosystemseng.2013.02.006

Tong JH, Jiang HY, Jiang ZH, Cui D, 2014. Experiment on parameter optimization of gripper needles clamping seedling plug for automatic transplanter. T CSAE 30 (16): 8-16.

Yang Y, Ting KC, Giacomelli GA, 1991. Factors affecting performance of sliding-needles gripper during robotic transplanting of seedlings. Am Soc Agr Eng 7 (4): 493-498. https://doi.org/10.13031/2013.26251

Zappala S, Helliwell JR, Tracy SR, Mairhofer S, Sturrock CJ, Pridmore T, Bennet M, Mooney SJ, 2013a. Effects of X-Ray dose on rhizosphere studies using X-ray computed tomography. Plos One 8 (6): e67250. https://doi.org/10.1371/journal.pone.0067250

Zappala S, Mairhofer S, Tracy S, Sturrock CJ, Bennet M, Pridmore T, Mooney SJ, 2013b. Quantifying the effect of soil moisture content on segmenting root system architecture in X-ray computed tomography images. Plant Soil 370: 35-45. https://doi.org/10.1007/s11104-013-1596-1

Zhao D, Xu MX, Liu GB, Yao X, Tuo DF, 2017. Quantification of soil aggregate microstructure on abandoned cropland during vegetative succession using synchrotron radiation-based micro-computed tomography. Soil Till Res 165: 239-246. https://doi.org/10.1016/j.still.2016.08.007